Normalization approaches for the descent search direction in isogeometric shape optimization

Wang, Zhen Pei; Abdalla, Mostafa; Turteltaub, Sergio

DOI
10.1016/j.cad.2016.06.002

Publication date
2017

Document Version
Accepted author manuscript

Published in
Computer-Aided Design

Citation (APA)
Wang, Z. P., Abdalla, M., & Turteltaub, S. (2017). Normalization approaches for the descent search direction in isogeometric shape optimization. *Computer-Aided Design*, *82*, 68-78. https://doi.org/10.1016/j.cad.2016.06.002

Normalization approaches for the descent search direction in isogeometric shape optimization

Zhen-Pei Wang[1], Mostafa Abdalla, Sergio Turteltaub

Faculty of Aerospace Engineering, Delft University of Technology, Kluyverweg 1, 2629 HS Delft, the Netherlands.

Abstract

In isogeometric shape optimization, the use of the search direction directly predicted from the discrete shape gradient makes the optimization history strongly dependent on the discretization. This discretization-dependency can affect the convergence and may lead the optimization process into a sub-optimal solution. The source of this discretization-dependency is traced to the lack of consistency with the local steepest descent search direction in the continuous formulation. In the present contribution, this inconsistency is analyzed using the shape variation equations and subsequently illustrated with a volume minimization problem. It is found that the inconsistency originates from the NURBS discretization which induces a discrete quadratic norm to represent the continuous Euclidean norm. To fix this inconsistency, three normalization approaches are proposed to obtain a discretization-independent normalized descent search direction. The discretization-independence of the proposed approaches is verified with a benchmark problem. The superiority of the proposed search direction and its suitability for numerical implementation is illustrated with examples of shape optimization for mechanical and thermal problems. The proposed methodology also applies to the ”mesh-dependency” in tradational FE-based shape optimization.

Keywords:
Isogeometric analysis, Shape optimization, Normalization approach,
Discretization-dependency, Mesh-dependency

1. Introduction

The recently developed isogeometric analysis (IGA) has been aimed from the start at integrating computer aided design (CAD) and analysis [1]. This synthesis of geometry and analysis has naturally led to renewed interest in developing structural shape optimization. The advantages of using isogeometric analysis in shape optimization are embodied in its ability to preserve exact CAD geometrical descriptions and its enhanced sensitivity analysis as explained in [2] and [3].

Isogeometric analysis is used for shape design optimization of curved beam structures in [4] and [5], vibrating membranes in [6], pulsatile ventricular assist devices in [7] and shells in [8] and [9]. Non-mechanical design optimization works are presented by [10] for photonic crystals, [11] for electromagnetic scattering problems, [12] for heat conduction problems, [13] and [14] for the

[1]Z.P.Wang@tudelft.nl

fluid problems. Shape optimization using a T-spline based isogeometric method is presented in [15]. Isogeometric shape optimization under time-varying loading conditions has recently been analyzed in [16]. The exact geometric description using IGA also provides a good opportunity to develop shape optimization using boundary element method [17]. A method to avoid mesh irregularity for the interior control points updating in isogeometric shape optimization is presented in [18].

Compared with shape optimization based on the traditional finite element method, isogeometric shape optimization can provide a simpler and more accurate sensitivity, especially when the sensitivity expressions depend on geometric properties such as curvature. This advantage is discussed in terms of enhanced sensitivity in the work of [3]. In the framework of NURBS discretization for design, full analytical sensitivities with respect to both the positions and the weights of NURBS control points are achievable [19]. Design sensitivity analysis is further studied using transformed basis functions for Kronecker delta property in the work of [20].

In isogeometric shape optimization, the control points, or some value associated with the control points, are commonly chosen as the design variables. The shape design sensitivity leads to the calculation of the discrete shape gradient with respect to control point variables. Depending on how a search direction is constructed from the discrete shape gradient, discretization-dependency of the optimization history might arise [9]. This discretization-dependency can affect the convergence speed and may lead the optimization process into a sub-optimal solution. It should be noted here that this discretization-dependency is not limited to shape optimization based on isogeometric analysis; it also occurs in shape optimization based on traditional FE-based shape optimization, which is often termed ”mesh-dependency” or ”parameterization-dependency” in the classical finite element formulation and leads to a zigzag boundary (see [21] and [22], etc.).

The discretization-dependency of the sensitivity analysis requires some technique to find a reasonable search direction. In [4], a Sobolev semi-norm, referred to as ”shape change norm”, is introduced to balance the shape variation with the cost of constructing the Sobolev semi-norm and solving a system of equations. In [23], the H^1 gradient method is used such that the discretization-dependency is avoided at the expense of solving a reshaping problem constructed by the H^1 gradient method. In [24], [25], [26] and [27], a similar method called ”traction method” is used to secure the shape regularity at about the same price as the H^1 gradient method. Other approaches and mesh regularization strategies, such as the filtering method, are presented for discretization-free shape optimization in [28], [21] and [29] to avoid the shape irregularity, referred to as a “parameterization-free” optimization. However, all of these approaches require to construct a system of linear equations and solve it. In [9], a ”sensitivity weighting” scheme is employed to obtain a discretization-independent search direction. The ”sensitivity weighting” is computationally much simpler since it only requires a locally integrated ’weighting’ factor over the local support of the corresponding design control point. While the ”sensitivity weighting” approach is shown to work in [9], the underlying reasons of its success and where the problem originates remain not clear.

The simplest and most intuitive search direction is the steepest descent direction. The use of the steepest descent direction, computed from the *discrete* shape gradient, makes the optimization history strongly dependent on the discretization. In this paper, we analyze the cause of the discretization-dependency of the steepest descent search direction from the underlying mathematical aspects and propose three normalization approaches to obtain a discretization-independent search direction, namely (i) a “standard” normalization, (ii) a diagonally-lumped mapping matrix (DLMM) normalization and (iii) a simplified DLMM normalization. The approaches proposed in the present contribution will also work for the finite element method based shape

optimization especially these methods using NURBS parameterization to describe the geometry (see, e.g., [30], [31], [32], [33] and [34]).

The paper is organized as follows: The isogeometric discretization framework is presented in Sec. 2 and the continuous and discrete gradients and search directions are shown in Sec. 3. The discretization-dependency of the un-normalized search direction is illustrated in Sec. 4 using a volume minimization problem with different NURBS discretizations. A quadratic norm induced by the NURBS discretization is derived in Sec. 5. Subsequently, a standard normalization approach for an optimization problem with a quadratic norm is proposed to obtain a discretization -independent search direction. Using the concept of the lumped mass matrix and the partition of unity property of NURBS, two simpler approaches are also proposed. The suitability of the normalization schemes is verified in Sec. 6 using the same volume minimization problem presented in Sec. 4 and, additionally, using the sensitivity analysis in a volume minimization problem of a two-dimensional domain. Design problems of a three-dimensional fillet and a two-dimensional thermal isolating panel are presented in Sec. 7 to demonstrate the superiority of the proposed normalization approaches. Concluding remarks are presented in Sec. 8.

2. Isogeometric discretization

The basic idea behind isogeometric analysis is to use NURBS, commonly used to describe the geometry, as the shape functions of the finite element analysis. A NURBS geometry can be treated as a mapping from a B-spline geometry by weight functions. A B-spline curve with a degree of p is defined as

$$\boldsymbol{x}[\xi] = \sum_{i=1}^{n} N^{i,p}[\xi]\boldsymbol{x}^i \qquad 0 \leqslant \xi \leqslant 1 \tag{1}$$

where $\boldsymbol{x}$ is the location of a point in the physical space corresponding to the parameter ξ defined in a parametric space, n is the number of the control points, $N^{i,p}$ is the ith basis function of degree p, and $\boldsymbol{x}^i$ is the location of the ith control point. The ith B-spline basis function of degree p can be defined as

$$\begin{aligned} N^{i,0}[\xi] &= \begin{cases} 1 & \text{if} \quad \xi_i \leqslant \xi < \xi_{i+1} \\ 0 & \text{otherwise} \end{cases} \\ N^{i,p}[\xi] &= \frac{\xi - \xi_i}{\xi_{i+p} - \xi_i} N^{i,p-1}[\xi] + \frac{\xi_{i+p+1} - \xi}{\xi_{i+p+1} - \xi_{i+1}} N^{i+1,p-1}[\xi], \quad [p > 0], \end{aligned} \tag{2}$$

where ξ_i is the ith element of a non-decreasing knot vector, i.e.,

$$\boldsymbol{\xi} = \{\xi_1, \xi_2, \xi_3, ..., \xi_{n+p+1}\}.$$

The knot vector is said to be *uniform* if the knots are equally spaced and *open* if the knots at each ends have $p + 1$ multiplicity, respectively. A uniform vector with $p + 1$ multiple equal knots at each end is referred to as *open-uniform*.

Adding a weight to each control point of a B-spline curve, it gives a NURBS curve with better flexibility. The basis function $R^{i,p}[\xi]$ for a pth degree NURBS curve is defined as

$$R^{i,p}[\xi] = \frac{N^{i,p}[\xi]w^i}{W[\xi]}, \tag{3}$$

where w^i is the weight of the ith control point and $W[\xi] := \sum_{j=1}^{n} N^{j,p}[\xi] w^j$. Following this, a NURBS curve can be defined as

$$\boldsymbol{x}[\xi] = \sum_{i=1}^{n} R^{i,p}[\xi] \boldsymbol{x}^i. \tag{4}$$

The NURBS basis function $R^{i,p}[\xi]$ is nonnegative and is nonzero only on the subinterval $[\xi_i, \xi_{i+p+1}]$. This property is referred to as *local support*, which implies that moving a control point $\boldsymbol{x}^i$ only affects the part of the geometry that corresponds to the subinterval $[\xi_i, \xi_{p+i+1}]$ in the parametric space. NURBS surfaces and volumes can be defined following the same way as

$$\boldsymbol{x}[\xi, \eta] = \sum_{i=1}^{n} \sum_{j=1}^{m} R^{ij}[\xi, \eta] \boldsymbol{x}^{ij}, \tag{5}$$

and

$$\boldsymbol{x}[\xi, \eta, \zeta] = \sum_{i=1}^{n} \sum_{j=1}^{m} \sum_{k=1}^{l} R^{ijk}[\xi, \eta, \zeta] \boldsymbol{x}^{ijk}, \tag{6}$$

where ξ, η and ζ are parameters in the parametric space and, for simplicity, the degrees of the functions is not shown. More details about NURBS can be found in [35]. By introducing a mapping function

$$I = \begin{cases} I[i], & \text{for 1D parametric space} \\ I[i, j], & \text{for 2D parametric space} \\ I[i, j, k], & \text{for 3D parametric space} \end{cases} \tag{7}$$

points in a region generated from NURBS can be expressed in a general way as

$$\boldsymbol{x} = \sum_{I} R^I[\boldsymbol{\chi}] \boldsymbol{x}^I = \boldsymbol{X}\boldsymbol{R}, \tag{8}$$

where $\boldsymbol{R} = [R^1, R^2, \cdots]$, $\boldsymbol{X} = [\boldsymbol{x}^1, \boldsymbol{x}^2, \cdots]$ and $\boldsymbol{\chi}$ is a vector-valued parameter equal to either ξ, (ξ, η) or (ξ, η, ζ) depending on the dimension of the parametric space. The meaning of the operation $\boldsymbol{X}\boldsymbol{R}$ is implicitly defined in (8).

Since the shape of a NURBS-generated object depends on the control points, these can be naturally used as design variables for shape optimization. Furthermore, the NURBS basis functions can also be used as shape functions for analysis, which is the underlying principle behind isogeometric analysis. Isogeometric shape optimization, which corresponds to the coupling between a geometrical design and an isogeometric analysis, uses NURBS discretization both for the design and analysis. With the NURBS discretization, the integral of a function f in a domain D in the physical space can be evaluated over the corresponding domain $\bar{D}$ in the parametric space, i.e.,

$$\int_D f[\boldsymbol{x}] \mathrm{d}D = \int_{\bar{D}} f[\boldsymbol{x}[\boldsymbol{\chi}]] \left|\boldsymbol{J}[\boldsymbol{\chi}]\right| \mathrm{d}\bar{D} \tag{9}$$

where $\boldsymbol{J}$ is the Jacobian matrix between the parametric space and the physical space and $|\boldsymbol{J}|$ is its norm or the absolute value of its determinant depending on the dimensions of the parametric and physical space (see, e.g., [36]).

3. Continuous and discrete shape gradients and search directions

3.1. Continuous shape gradient and search direction

A typical shape optimization problem can be formulated as the minimization of a given objective functional Ψ, which may depend on a field $\boldsymbol{u}$ and/or its gradient $\nabla\boldsymbol{u}$ defined in a domain $\Omega \in \mathbb{R}^d$, i.e.,

$$\Psi = \int_{\Omega} F(\boldsymbol{u}, \nabla\boldsymbol{u}, \boldsymbol{x})\mathrm{d}\Omega, \tag{10}$$

where F is the objective density function, which may also explicitly depend on the location $\boldsymbol{x}$. The minimization is carried out over a set of admissible domains Ω. A gradient-based descent algorithm requires expressing the variation $\delta\Psi$ of the objective functional with respect to the design variables. Given a domain D that may corresponds to Ω or its boundary Γ in physical space depending on whether the domain or the boundary integral approach is used for continuous sensitivity analysis, in a *continuous* formulation, the design variables are points $\boldsymbol{x} \in D$ and the variation can be expressed as

$$\delta\Psi = \langle \boldsymbol{g}, \delta\boldsymbol{x} \rangle_D = \int_D \boldsymbol{g} \cdot \delta\boldsymbol{x}\, \mathrm{d}D, \tag{11}$$

where $\delta\boldsymbol{x}$ represents the variation of $\boldsymbol{x}$ and $\boldsymbol{g} = \boldsymbol{g}[\boldsymbol{x}]$ denotes the local shape gradient (see, e.g., [16]) and $\langle \cdot, \cdot \rangle_D$ is a conveniently-chosen inner product over the integration domain D. An alternative representation of $\delta\boldsymbol{x}$ is to express it in terms of so-called design velocity, i.e., $\delta\boldsymbol{x} = \boldsymbol{v}\delta s$, where s is a time-like parameter and $\boldsymbol{v} = \mathrm{d}\boldsymbol{x}/\mathrm{d}s$ is the design velocity (see [16]).

The product used in the integrand in (11) is the canonical Euclidean inner product in $\mathbb{R}^d$. Correspondingly, given an arbitrary search direction $\delta\boldsymbol{x}$, the local *continuous steepest descent search direction* $\boldsymbol{d}_c$ (or *analytical* search direction), which coincides with the negative of the continuous shape gradient, at a location $\boldsymbol{x}$ is

$$\boldsymbol{d}_c = -\boldsymbol{g} \ \text{[Continuous]}. \tag{12}$$

With the continuous steepest descent search direction, functional Ψ decreases in the fastest direction by

$$\delta\Psi|_{\delta\boldsymbol{x}=\boldsymbol{d}_c} = -\int_D \boldsymbol{d}_c \cdot \boldsymbol{d}_c \, \mathrm{d}D \, . \tag{13}$$

Using (12), the design domain may be updated in an iterative descent algorithm from (iteration s to iteration $s+1$) as

$$\boldsymbol{x}^{(s+1)} = \boldsymbol{x}^{(s)} + \alpha\boldsymbol{d}_c = \boldsymbol{x}^{(s)} - \alpha\boldsymbol{g}, \tag{14}$$

where α is a step size. For a suitably-chosen step size, (13) guarantees that the functional Ψ decreases if $\boldsymbol{x}$ is changed according to (14).

3.2. Discrete shape gradient and search direction

The above updating scheme is based on the continuous formulation (i.e., on the continuous descent direction $-\boldsymbol{g}$). For the actual numerical implementation, the geometry needs to be discretized according to (8). The discrete variation of the functional Ψ corresponds to a change due

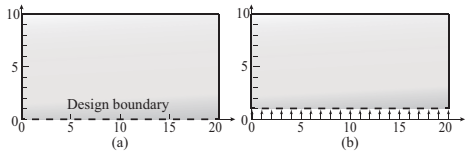

Figure 1 (a) 2D rectangular plate and its design boundary; (b) shape update using local steepest descent search direction $\boldsymbol{d}_c$ with one unit step size

to variations $\delta \boldsymbol{x}^I$ of the control points, which are the design variables in the discretized formulation. Substituting (8) into (11), the discrete variation can be obtained as

$$\delta\Psi = \int_D \boldsymbol{g} \cdot \sum_I R^I \delta \boldsymbol{x}^I \, \mathrm{d}D = \sum_I \boldsymbol{g}_d^I \cdot \delta \boldsymbol{x}^I = \boldsymbol{G}_d \cdot \delta \boldsymbol{X}, \tag{15}$$

where $\boldsymbol{G}_d := \left[\boldsymbol{g}_d^1, \boldsymbol{g}_d^2, \cdots\right]$, $\delta \boldsymbol{X} = \left[\delta \boldsymbol{x}^1, \delta \boldsymbol{x}^2, \cdots\right]$ and $\boldsymbol{g}_d^I$ is the discrete shape gradient calculated from the continuous sensitivity analysis, i.e.,

$$\boldsymbol{g}_d^I = \langle \boldsymbol{g}, R^I \rangle_D = \int_D \boldsymbol{g} R^I \, \mathrm{d}D. \tag{16}$$

The discrete shape gradient $\boldsymbol{g}_d^I$ can also be calculated from a discrete sensitivity analysis approach (discretion-first approach), which is identical with the one calculated from above continuous approach.

When using the steepest descent method, it is often to directly use the negative of the discrete gradient as the *discrete search direction* $\boldsymbol{D}_d = \{\boldsymbol{d}_d^1, \boldsymbol{d}_d^2, \cdots\}$, i.e.,

$$\boldsymbol{D}_d = -\boldsymbol{G}_d, \qquad \text{[Discrete]}, \tag{17}$$

and the model is correspondingly updated by relocating the control points $\boldsymbol{x}^I$ as

$$\left(\boldsymbol{x}^I\right)^{(s+1)} = \left(\boldsymbol{x}^I\right)^{(s)} + \alpha \boldsymbol{d}_d^I = \left(\boldsymbol{x}^I\right)^{(s)} - \alpha \boldsymbol{g}_d^I \tag{18}$$

which implies that a typical point $\boldsymbol{x}$, in view of (8), is updated as

$$\boldsymbol{x}^{s+1} = \boldsymbol{x}^s + \alpha \sum_I \boldsymbol{d}_d^I R^I = \boldsymbol{x}^s + \alpha \boldsymbol{D}_d \boldsymbol{R} \, . \tag{19}$$

As can be seen from (16), the shape gradient $\boldsymbol{G}_d$ is highly dependent on the isogeometric discretization, which means the search direction is also discretization-dependent. This discretization -dependent search direction, henceforth referred to as the *un-normalized discrete search direction*, leads to discretization-dependent evolution of the design that, in turn, may lead to sub-optimal shape designs.

4. Discretization-dependency

The discretization-dependency may be illustrated by a volume minimization problem. For a domain Ω with boundary Γ, the volume of the domain can be expressed as

$$\Sigma = \int_\Omega \mathrm{d}\Omega. \tag{20}$$

Table 1 Different discretizations of the rectangular plate model, where $\boldsymbol{x}(x, y)$ is the location of the control points; $\boldsymbol{w}$ are the weights of the control points; $\boldsymbol{\xi}$ and $\boldsymbol{\eta}$ are knot vectors

Cases	Discretizations
1	$\boldsymbol{x}_{\|y=0,5,10} = \{0, 4, 8, 12, 16, 20\}$ $\boldsymbol{w}_{\|y=0,5,10} = \{1, 1, 1, 1, 1, 1\}$ $\boldsymbol{\xi} = \{0\ 0\ 0\ 0.25\ 0.5\ 0.75\ 1\ 1\ 1\ \}$ $\boldsymbol{\eta} = \{0\ 0\ 0\ 1\ 1\ 1\ \}$
2	$\boldsymbol{x}_{\|y=0,5,10} = \{0, 4, 8, 12, 16, 20\}$ $\boldsymbol{w}_{\|y=0,5,10} = \{1, 1, 1, 1, 1, 1\}$ $\boldsymbol{\xi} = \{0\ 0\ 0\ 0.1\ 0.2\ 0.3\ 1\ 1\ 1\ \}$ $\boldsymbol{\eta} = \{0\ 0\ 0\ 1\ 1\ 1\ \}$
3	$\boldsymbol{x}_{\|y=0,5,10} = \{0, 4, 8, 12, 16, 20\}$ $\boldsymbol{w}_{\|y=5,10} = \{1, 1, 1, 1, 1, 1\}$ $\boldsymbol{w}_{\|y=0} = \{1, 1, 0.6, 0.6, 1, 1\}$ $\boldsymbol{\xi} = \{0\ 0\ 0\ 0.25\ 0.5\ 0.75\ 1\ 1\ 1\ \}$ $\boldsymbol{\eta} = \{0\ 0\ 0\ 1\ 1\ 1\ \}$
4	$\boldsymbol{x}_{\|y=0,5,10} = \{0, 3, 5, 6, 14, 20\}$ $\boldsymbol{w}_{\|y=0,5,10} = \{1, 1, 1, 1, 1, 1\}$ $\boldsymbol{\xi} = \{0\ 0\ 0\ 0.25\ 0.5\ 0.75\ 1\ 1\ 1\ \}$ $\boldsymbol{\eta} = \{0\ 0\ 0\ 1\ 1\ 1\ \}$
5	finite element (FE) discretization: $\boldsymbol{x} = \{0, 3, 5, 7, 10, 13, 15, 17, 20\}$ $\boldsymbol{y} = \{0, 5, 10\}$

Using Reynolds transport theorem, the variation of the volume via a boundary integral approach can be obtained as

$$\delta\Sigma = \int_{\Gamma} \boldsymbol{n} \cdot \delta\boldsymbol{x} \mathrm{d}\Gamma, \tag{21}$$

where $\boldsymbol{n}$ is the unit outward normal vector(see, e.g., [16]). In this case, the continuous local shape gradient is simply

$$\boldsymbol{g} = \boldsymbol{n}. \tag{22}$$

To clearly illustrate the influence of the discretization on the search direction, it is useful to start from a simple geometry, namely a rectangular domain as shown in Fig. 1(a), and to consider only the bottom boundary as the design boundary. In this case, a step to minimize the volume, based on the continuous steepest descent search direction in (14) with the gradient (22), consists on simply "moving" the bottom boundary uniformly upwards, as shown in Fig. 1(b) (i.e., moving the boundary in the opposite direction of the outward unit vector). Ideally, a discrete search direction should provide a good approximation to this behavior.

If the domain is discretized by NURBS, the shape gradient with respect to the location of the I-th control point, $\boldsymbol{x}^I$, is

$$\boldsymbol{g}_d^I = \int_{\Gamma} \boldsymbol{n} R^I \, \mathrm{d}\Gamma. \tag{23}$$

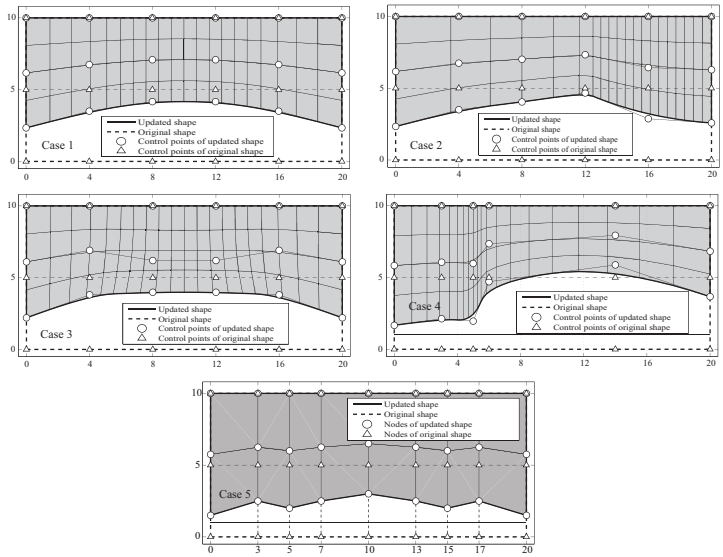

Figure 2 The shape update for different cases with the un-normalized search direction

Five different discretizations of the rectangular model are shown in Table 1. In case 1, the control points are uniformly distributed in the physical space. The knot vector $\boldsymbol{\xi}$ and $\boldsymbol{\eta}$ are open -uniform. The weights of the control points have all the same value of 1. Case 2 has have the same control points and weights, but its knot vector $\boldsymbol{\xi}$ is non-uniform. Case 3 has the same control points and knot vectors, but two control points at $x = 8$, $y = 0$ and $x = 12$, $y = 0$ have the weights reduced to 0.6. Case 4 has the same knot vectors and weights, but the control points are not uniformly distributed in the physical space. Case 5 is simply a linear finite element discretization.

The design shape, updated based on (19) with search direction (17) and a step size $\alpha = 1$, is shown in Fig. 2. The locations of the interior control points are interpolated from the locations of boundary control points. It can be seen that the updated shape is strongly dependent on the discretization and is *not* consistent with the continuous steepest search direction shown in Fig. 1(b). It also shows that the discretization-dependency also happens to the finite element discretization.

In the context of NURBS, the problems generated from the discretization-dependency are attributable to the following aspects/factors:

- non-uniform property of the knot vector in parametric space, which is illustrated by case 2
- weights of the design control points, which is illustrated by case 3
- non-uniform local support in physical space, which is illustrated by case 4

Case 1, like case 4, also illustrates the effect of the non-uniform local support, which originates from the support of the shape functions on the left and right ends. The problems generated by the un-normalized search direction can be corrected using various alternative approaches, as addressed in the next section.

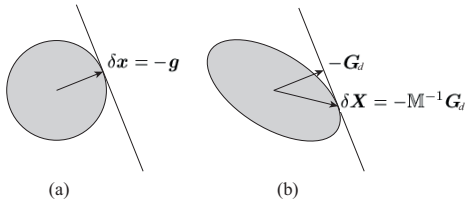

Figure 3 Illustration of steepest descent directions for (a) Euclidean norms and (b) quadratic norms. The ball in (a) is the unit ball of the Euclidean norm, translated to point $\boldsymbol{x}$. The ellipsoid in (b) represents the unit ball of the quadratic norm and the steepest descent direction $\delta \boldsymbol{X}$ corresponds to the largest distance inscribed in the ellipse (see, e.g., [37] for details)

5. Normalization of the search directions

The reason for the discretization-dependency is that the un-normalized discrete search direction $\boldsymbol{D}_d$ is not consistent with the continuous steepest search direction $\boldsymbol{d}_c$.

5.1. Consistent discretization

In order to well approximate the continuous steepest descent search direction $\boldsymbol{d}_c$ and eliminate the discretization-dependency, the *normalized search direction* $\boldsymbol{D}_n = \{\boldsymbol{d}_n^1,\ \boldsymbol{d}_n^2,\ \cdots\}$ is introduced such that

$$\boldsymbol{d}_c \approxeq \sum_J R^J \boldsymbol{d}_n^J = \boldsymbol{D}_n \boldsymbol{R}. \tag{24}$$

Using (24) in (13) implies that

$$\delta\Psi|_{\delta \boldsymbol{X} = \boldsymbol{D}_n} = -\sum_I \sum_J \int_D R^I R^J \,\mathrm{d}D \left(\boldsymbol{d}_n^I \cdot \boldsymbol{d}_n^J\right) = -\boldsymbol{M}\boldsymbol{D}_n \cdot \boldsymbol{D}_n, \tag{25}$$

where $\boldsymbol{M}$ is a second-order symmetric mass matrix-like mapping defined as

$$\boldsymbol{M} = \boldsymbol{M}^{\mathrm{T}} := \int_D \boldsymbol{R} \otimes \boldsymbol{R} \,\mathrm{d}D. \tag{26}$$

The interpretation of the tensor product $\otimes$ can be obtained from (25) and (26).

5.2. Standard normalization

From (13), it can be seen that the variation of the objective functional in the continuous sense is a Euclidean norm. The steepest descent direction of an Euclidean norm is simply the negative gradient, which is defined in (12). Nevertheless, from (25) it can be seen that once the continuous steepest search direction is discretized, the variation of the objective functional becomes a (squared) quadratic norm. For problems with quadratic norms, a normalization approach is required to obtain the steepest descent direction. The steepest descent direction for Euclidean and quadratic norms are illustrated in Fig.3. A detailed explanation of this can be found in [37].

Using equations (15) and (25), it follows that

$$-\boldsymbol{M}\boldsymbol{D}_n \cdot \boldsymbol{D}_n = \boldsymbol{G}_d \cdot \boldsymbol{D}_n. \tag{27}$$

Following this, the *normalized search direction*, which is the *discrete steepest search direction* corresponding to the quadratic norm, can be obtained as

$$\boldsymbol{D}_n = \boldsymbol{M}^{-1}\boldsymbol{D}_d, \quad \text{[Standard normalization]}, \tag{28}$$

which is the standard way to obtain normalized search direction. This standard approach, however, requires computing the mapping tensor $\boldsymbol{M}$ and solving (28).

5.3. Diagonally-lumped mapping matrix (DLMM) normalization

A computationally-attractive alternative to the standard approach is to introduce the *diagonally lumped mapping matrix* (DLMM), denoted $\bar{\boldsymbol{M}}$, such that the diagonal components are

$$\bar{\boldsymbol{M}}_{II} := \sum_J \boldsymbol{M}_{IJ}\,, \tag{29}$$

and the off-diagonal components are zero. From the partition of unity property, i.e., $\sum_J R^J = 1$, and in view of (26) and (29), it follows that

$$\bar{\boldsymbol{M}}_{II} = \int_D R^I \,\mathrm{d}D\,. \tag{30}$$

The advantage of approximating $\boldsymbol{M}$ with $\bar{\boldsymbol{M}}$ is that a normalized search direction can simply be computed as

$$\boldsymbol{d}_n^I = -\frac{\boldsymbol{g}_d^I}{\bar{\boldsymbol{M}}_{II}} = -\frac{\int_D \boldsymbol{g} R^I \,\mathrm{d}D}{\int_D R^I \,\mathrm{d}D} \quad \text{[DLMM normalization]}\,. \tag{31}$$

This type of approach is referred to as "sensitivity weighting" in [9].

5.4. Simplified DLMM normalization

The DLMM approach is defined in the physical space. As mentioned in Sec.4, the discretization-dependency of the search direction is attributed to the weights and the non-uniformity of the local support in parametric and physical space. If the "sensitivity weighting" is done only in the parametric space, the dependency on the local support in the physical space vanishes naturally. This observation motivates the development of a simplified approach where the normalization is carried out in the NURBS parametric space. For the DLMM normalization, the search direction (31), integrated in physical space D, can be expressed in parametric space $\bar{D}$ as

$$\boldsymbol{d}_n^I = -\frac{\int_{\bar{D}} \boldsymbol{g} R^I |\boldsymbol{J}| \,\mathrm{d}\bar{D}}{\int_{\bar{D}} R^I |\boldsymbol{J}| \,\mathrm{d}\bar{D}}\,. \tag{32}$$

The NURBS geometry can be treated as a mapping from the corresponding B-splines model via weighted functions (see (3)). The "sensitivity weighting" can be also simply carried out in the B-spline parametric space by mapping the NURBS space back to the B-spline space, which is independent on the weights of the control points. Towards developing a simplified method, the DLMM normalization is further approximated as

$$\boldsymbol{d}_n^I \approx -\frac{\int_{\bar{D}} \boldsymbol{g} N^I \,\mathrm{d}\bar{D}}{\int_{\bar{D}} N^I \,\mathrm{d}\bar{D}}\,. \tag{33}$$

Implicitly, it is assumed that the mean contributions of the Jacobian $\boldsymbol{J}$ and the weight W are compensated in the ratio (33). The rationale is that, based on the mean value theorem, if the upper and lower bounds of the Jacobian $|\boldsymbol{J}|$ and the weight W are relatively close to each other in the domain of integration then their contribution in the numerator will be compensated with that of the denominator, i.e., since $R^I = w^I N^I / W$,

$$\frac{\int_{\bar{D}} \boldsymbol{g} w^I N^I |\boldsymbol{J}|/W \, \mathrm{d}\bar{D}}{\int_{\bar{D}} w^I N^I |\boldsymbol{J}|/W \, \mathrm{d}\bar{D}} \approx \frac{(|\boldsymbol{J}|/W)^* \int_{\bar{D}} \boldsymbol{g} N^I \, \mathrm{d}\bar{D}}{(|\boldsymbol{J}|/W)^{**} \int_{\bar{D}} N^I \, \mathrm{d}\bar{D}} \tag{34}$$

where $(|\boldsymbol{J}|/W)^*$ and $(|\boldsymbol{J}|/W)^{**}$ correspond to ratios of the Jacobian and the weight, each evaluated at some point in the domain of integration. The implicit assumption that we use is that $(|\boldsymbol{J}|/W)^* \approx (|\boldsymbol{J}|/W)^{**}$. The effect of this assumption on the search direction is tested in the next section, but first it is useful to explore the computational advantages of the expression (33).

Using the property of *unity of integral* [38] of B-spline basis

$$\frac{\int N^{i,p} \mathrm{d}\xi}{\xi_{i+p+1} - \xi_i} = \frac{1}{p+1}, \tag{35}$$

Equation (33) can be expressed as

$$\boldsymbol{d}_n^I = -\frac{(p+1) \int_{\bar{D}} \boldsymbol{g} N^I \, \mathrm{d}\bar{D}}{\xi_{i+p+1} - \xi_i}, \quad \text{[Simplified DLMM]} \tag{36}$$

with the index $I = I(i)$ given by (7) (with the corresponding degree p) in the one-dimensional case. Observe that the simplified DLMM normalization only requires one integration over the B-spline space.

Following (5) and (6), (35) can be easily extended to the 2D and 3D parametric space, respectively, as

$$\frac{\int\int N^{i,p}[\xi] N^{j,q}[\eta] \mathrm{d}\xi \mathrm{d}\eta}{\left(\xi_{i+p+1} - \xi_i\right)\left(\eta_{j+q+1} - \eta_j\right)} = \frac{1}{(p+1)(q+1)} \tag{37}$$

and

$$\frac{\int\int\int N^{i,p}[\xi] N^{j,q}[\eta] N^{k,r}[\zeta] \mathrm{d}\xi \mathrm{d}\eta \mathrm{d}\zeta}{\left(\xi_{i+p+1} - \xi_i\right)\left(\eta_{j+q+1} - \eta_j\right)\left(\zeta_{k+r+1} - \zeta_k\right)} = \frac{1}{(p+1)(q+1)(k+1)}. \tag{38}$$

The superscripts q and r are the degrees of the NURBS basis for parameters η and ζ, respectively. Following (37) and (38), the simplified DLMM approach for the 2D and 3D parametric spaces can be obtained, respectively, as

$$\boldsymbol{d}_n^I = -\frac{(p+1)(q+1) \int_{\bar{D}} \boldsymbol{g} N^I \, \mathrm{d}\bar{D}}{\left(\xi_{i+p+1} - \xi_i\right)\left(\eta_{j+q+1} - \eta_j\right)} \tag{39}$$

and

$$\boldsymbol{d}_n^I = -\frac{(p+1)(q+1)(k+1) \int_{\bar{D}} \boldsymbol{g} N^I \, \mathrm{d}\bar{D}}{\left(\xi_{i+p+1} - \xi_i\right)\left(\eta_{j+q+1} - \eta_j\right)\left(\zeta_{k+r+1} - \zeta_k\right)}, \tag{40}$$

with the index I given by (7) for the two- and three-dimensional cases, respectively. The computational advantage of the simplified DLMM approach is that (i) it does not require to (numerically) solve problem (28) and (ii) it takes advantage of closed-form expressions of integrals of B-splines.

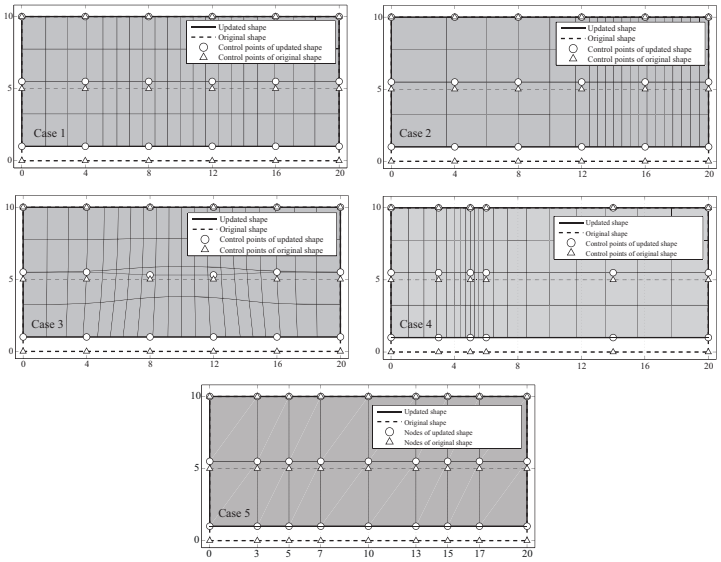

Figure 4 Shape updates for cases 1 to 5 using the simplified DLMM normalization approach

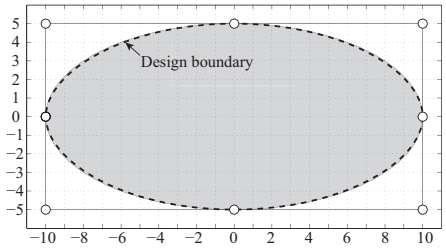

Figure 5 Volume minimization problem of an elliptic plate

6. Verification

6.1. Volume minimization of an initially rectangular domain

The approaches presented in Sec. 5 were verified using the same volume minimization problem with the four different discretizations cases presented in Sec. 4, namely using an initially rectangular domain. It was found that, for all cases, all normalization approaches generated the same normalized search direction $(0, 1)$, to within the same numerical tolerance, which is consistent with the continuous one. The shape updates of the four different discretizations with the normalized search direction are shown in Fig. 4, from which it can be seen that the shape updates indeed match the continuous solution shown in Fig. 1(b). Case 5 also shows that the normalization approaches can be generally applicable to the FE-based shape optimization.

6.2. Volume minimization of an initially elliptic plate

To further test the normalization approach in the context of a variable curvature, consider an elliptical region as shown in Fig. 5. The boundary of the region is discretized with the control

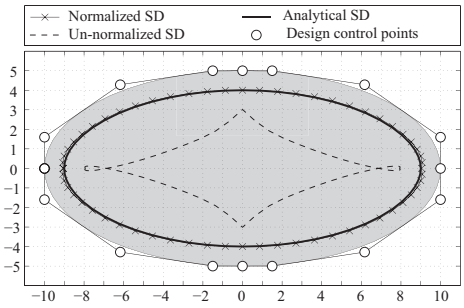

Figure 6 Shape updates using (i) un-normalized search direction (SD), (ii) continuous local steepest descent (analytical) search direction and (iii) the normalized search direction (simplified DLMM), all with a step size $\alpha = 1$

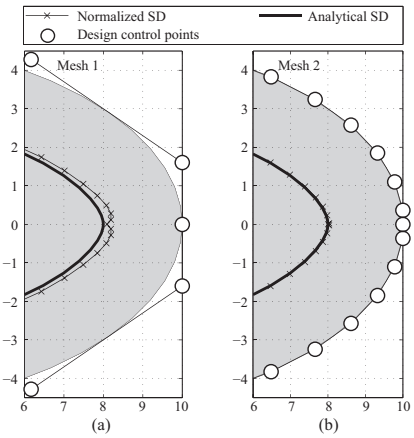

Figure 7 Shape updates using (i) the continuous local steepest descent (analytical) search direction and (ii) the normalized search direction (simplified DLMM) with a step size $\alpha = 2$ for two different meshes

Table 2 The L^2 norm of the error between the analytical and normalized search direction for mesh 1 and mesh 2 using the different normalization approaches

Mesh	Approach		
	Standard	DLMM	Simplified DLMM
1	0.02121	0.02597	0.02476
2	0.02087	0.02140	0.02129

points shown in Fig. 5 and a knot vector $\boldsymbol{\xi} = \left[0, 0, 0, \frac{1}{4}, \frac{1}{4}, \frac{1}{2}, \frac{1}{2}, \frac{3}{4}, \frac{3}{4}, 1, 1, 1\right]$. For design purposes, the model was refined using the knot vectors $\boldsymbol{\xi} \cup \boldsymbol{\xi}'$ and $\boldsymbol{\xi} \cup \boldsymbol{\xi}''$, with $\boldsymbol{\xi}'$ corresponding to a partition of $[0, 1]$ in subintervals of length 0.1 and $\boldsymbol{\xi}''$ a partition of $[0, 1]$ in subintervals of length 0.025. These two knot vectors are referred to as *mesh 1* and *mesh 2*, respectively.

For mesh 1, the shape updates using (i) the un-normalized search direction, (ii) the continuous steepest (analytical) search direction and (iii) the discrete steepest (normalized) search direction (using the simplified DLMM method), all with a step size $\alpha = 1$, are plotted in Fig. 6. The shape updates using the standard and the DLMM normalization where visually overlapping with the simplified DLMM update, hence, for clarity, they are not included in the figure. It can be seen from Fig. 6 that the shape update using the normalized search direction is very close to the one using the analytical search direction defined in (12), while the one using the un-normalized search direction has a large discrepancy with the analytical solution and, in fact, the shape becomes inadmissible. In spite of the fact that the normalized search direction can approximate the analytical one relatively well, naturally there is an intrinsic error due to the discretization. This discrepancy can be particularly observed in the region of maximum curvature as indicated in Fig. 7, which shows the updated shape for (a) mesh 1 and (b) mesh 2 using the normalized search direction. To clearly visualize the discrepancy between the numerical and analytical search directions, the updated shapes are plotted using a larger step size, namely $\alpha = 2$. Comparing Fig. 7(a) and Fig. 7(b) it is clear that the numerical error can be reduced by a refinement of the design model leading to a more accurate updated geometry. To quantify the discrepancy between the distinct normalization approaches the L^2 norm of the error between the analytical and normalized search direction for mesh 1 and mesh 2 using the different normalization approaches is presented in Tab.2.

From Tab.2, it can be quantitatively seen that the mesh refinement reduces the approximation. It can also be observed that, the standard normalization approach provides a slightly more accurate search direction compared with the lumped-matrix-based approaches (DLMM and simplified DLMM). However, both lumped-matrix-based normalization approaches provide an approximation comparable to the one obtained from the standard normalization. But they are computationally more efficient and simpler to implement, which justifies their use, particularly for problems with a large number of design variables.

7. Performance of normalization approach

In order to provide more insight on the effect of the normalization approach, two optimization problems are presented in this section. The first one is a mechanical problem where the objective is to reduce stress concentrations and the second is a thermal isolation problem where

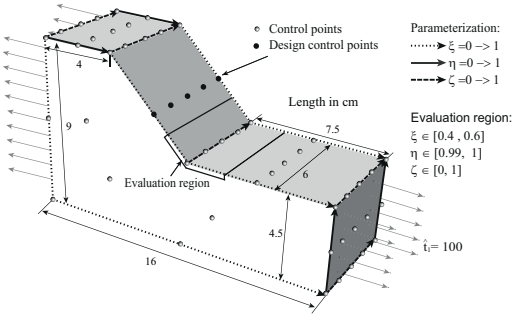

Figure 8 3D fillet model under tension

the objective is to minimize the net heat flux. In both problems, the solutions obtained with and without a normalized search direction are compared.

7.1. 3D fillet shape design optimization

Consider a 3D fillet under axial tension, as is shown in Fig. 8. The model is represented with NURBS and the correspondence between the parametric and the physical space is shown in Fig. 8. The region occupied by the fillet is denotes as Ω. In order to reduce the stress concentration at the transition corner, an objective function is defined over a local evaluation region $\Omega_\omega \subset \Omega$ as

$$\Psi_\omega = \int_\Omega \omega(\sigma_{\mathrm{v}} - \check{\sigma}_{\mathrm{v}})^2 \mathrm{d}\Omega \tag{41}$$

where the function σ_{v} is the Von Mises stress, ω is the characteristic function that has a value of 1 in Ω_ω and 0 outside of Ω_ω and $\check{\sigma}_{\mathrm{v}}$ is the mean Von Mises stress of the local domain Ω_ω, i.e.,

$$\check{\sigma}_{\mathrm{v}} = \frac{1}{\Omega_\omega} \int_{\Omega_\omega} \sigma_{\mathrm{v}} \mathrm{d}\Omega \,. \tag{42}$$

The local evaluation region Ω_ω is located around the transition corner, as is shown in Fig. 8. The characteristic function is defined in the parametric space as

$$\omega[\xi, \eta, \zeta] = \begin{cases} 1, \ 0.4 \le \xi \le 0.6, \ 0.99 \le \eta \le 1, \ 0 \le \zeta \le 1 \\ 0, \ \text{otherwise.} \end{cases}$$

As is also shown in Fig. 8, five control points were chosen as the discrete design variables. The objective was to minimize the difference between the local stress and the mean stress, so that the local stress concentration could be reduced. The sensitivity analysis, which was done using continuous adjoint method, can be found in [16] (see also [39]).

The iteration histories of the objective functional and the maximum stress are shown in Fig. 9, in which step 0 represents the initial design. The optimization process without the normalization approach converged after 11 steps with the maximum Von Mises stress reduced to about 150 MPa, while the process with the normalization approach started to converge with only 6 steps and the maximum Von Mises stress was reduced to about 130 MPa. The normalization approach used in this problem was the simplified DLMM approach. Fixed step sizes were used in this problem. The step sizes were chosen based on a parametric analysis that chooses distinct step

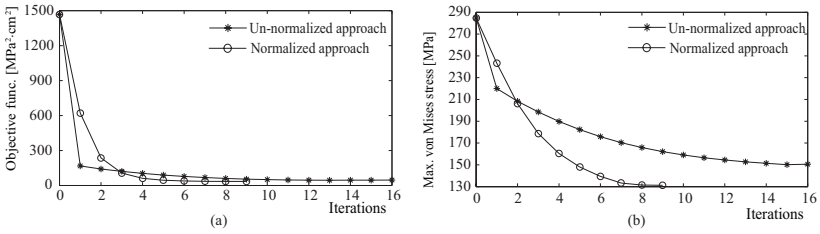

Figure 9 Iteration history of (a) objective functional and (b) maximum Von Mises stress

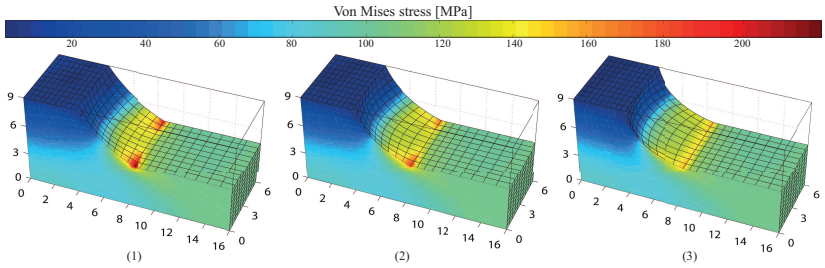

Figure 10 Shape updates without normalization approach at: (1) step 2, (2) step 6 and (3) step 16 (optimal)

sizes for the best performance (i.e., the "best" constant step size for each descent direction). The "best" constant step sizes for the normalized and un-normalized cases turned out to be 1×10^{-3} and 4×10^{-4}, respectively. It can clearly be seen that, even though the objective and maximum stress of the process without normalization approach decreased much faster than those of the one with normalization approach at the first step, the optimization with normalization approach still converged much faster and better.

The shape updates of steps 2 and 6 and the final step are plotted in Fig. 10 and Fig. 11, respectively. As can be seen from Fig. 10, in the design optimization process without normalization, the shape updating in the middle was bigger than the two sides, which resulted in a sub-optimal solution. In contrast, in the design process using the normalization approach shown in Fig. 11, all of the design control points moved uniformly, which overall provided a better convergence (i.e., fewer iterations for the same tolerance) and better performance of the optimal design.

7.2. Heat conduction problem

Consider a panel that separates two environments with a difference in temperature of 300°C as shown in Fig. 12. The bottom side of the panel is exposed to an ambient temperature of 300°C while the top side is exposed to an ambient temperature of 0°C. Heat is exchanged on both sides through convection. The convection coefficient of these two convective boundaries is 50 W/(m^2·°C). The thermal conductivity coefficient of the material used in the panel is 0.05 W/(m·°C). The original design has a dimension of 0.01 m $\times$ 0.04 m, which was originally dis-

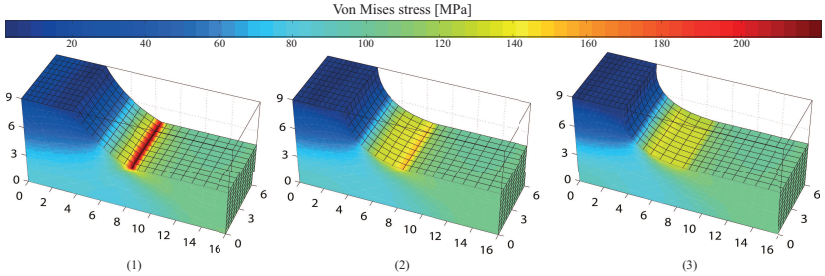

Figure 11 Shape updates with normalization approach at: (1) step 2, (2) step 6 and (3) step 9(optimal)

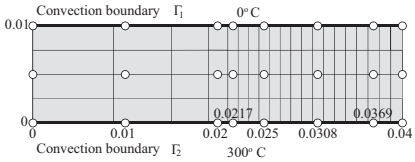

Figure 12 Thermal isolating panel with two convection boundaries and given ambient temperatures

cretized as

$$\begin{aligned}
&\boldsymbol{x}_{|y=0,0.005,0.01} = \{0, 0.01, 0.02, 0.03, 0.04\};\\
&\boldsymbol{w}_{|y=0,0.005,0.01} = \{1, 1, 1, 1, 1\};\\
&\boldsymbol{\xi} = \{0\ 0\ 0\ 0.1\ 0.2\ 1\ 1\ 1\ \};\\
&\boldsymbol{\eta} = \{0\ 0\ 0\ 1\ 1\ 1\ \}.
\end{aligned} \tag{43}$$

Using this structure, the optimization problem is to provide maximum insulation. The problem can be formulated with the objective to minimize the net heat flux Ψ on the top boundary under steady state conditions, where

$$\text{Minimizing } \Psi := \int_{\Gamma_1} h(\theta - \theta_{\text{top}}) \mathrm{d}\Gamma\,, \tag{44}$$

where h is the convection coefficient, θ is the temperature on Γ_1 and $\theta_{\text{top}} = 0°\text{C}$ is the ambient temperature on the top side. To prevent a trivial solution, which corresponds to an infinitely thick panel, a resource constraint is included, namely

$$\int_{\Omega} \mathrm{d}\Omega \leq 0.02 \times 0.04\,. \tag{45}$$

In the design space, the knot vector $\boldsymbol{\xi}$ is refined into $\boldsymbol{\xi} = \{0\ 0\ 0\ 0.1\ 0.2\ 0.25\ 0.5\ 0.75\ 1\ 1\ 1\ \}$ using h-refinement. The corresponding control points of the refined discretization are shown in Fig. 12. The sensitivity analysis, which was done using the continuous adjoint method, can be found in [12]. A descent method with a fixed step size was used in the iterative procedure. The step sizes used in this problem for the normalized and un-normalized cases are 5×10^{-9} and

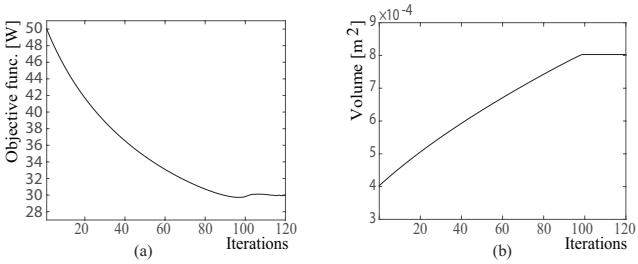

Figure 13 Iteration history of (a): objective function and (b): volume constraint without the normalization approach

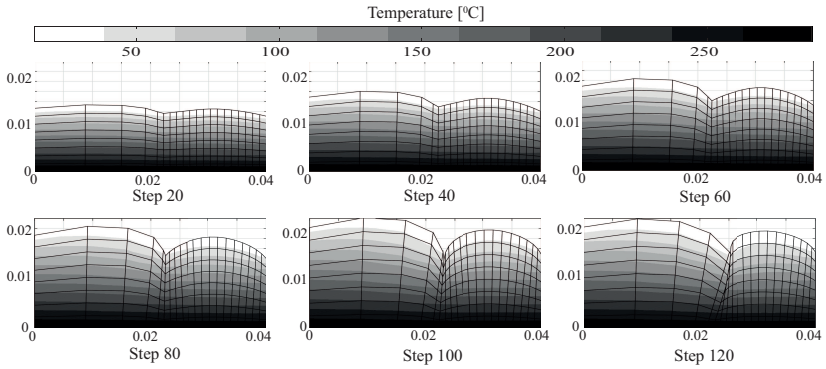

Figure 14 Evolution of the design shape without the normalization approach at selected steps throughout the optimization process and the corresponding temperature contour plot

3×10^{-7}, respectively. The reason that the step-size of the un-normalized case is bigger than the normalized one is due to the normalization factor $\int_D R^I \mathrm{d}D < 1$.

The ideal updating scheme for the structure is simply to increase the thickness *uniformly* until a global volume constraint becomes active (i.e., the volume reaches a maximum allowed value). The iteration history of the optimization process without the normalization approach, with a relatively small step size, is presented in Fig. 13. From the figure it can be seen that even with a small step size, the optimization was *not* able to converge. The evolution of the shape, at selected steps throughout the iterative process, is shown in Fig. 14. From the figure, it can be seen that the mesh distortion became severe after about 100 steps, preventing the descent method from converging.

In contrast, the optimization process with the normalization approach reached the volume constraint after 7 iteration steps, which was much faster than the case without normalization. The iteration history is shown in Fig. 15 and the design shapes at selected steps are plotted in Fig. 16. It can be clearly observed in Fig. 16 that using the normalized shape gradient resulted in intermediate designs consistently updated compared to the continuous case.

The mechanical and thermal examples shown in this section illustrate the relevance of a consistent approximation of the search direction in terms of overall *efficiency* and *convergence*. Although the normalized search direction requires a (small) additional computational effort, the

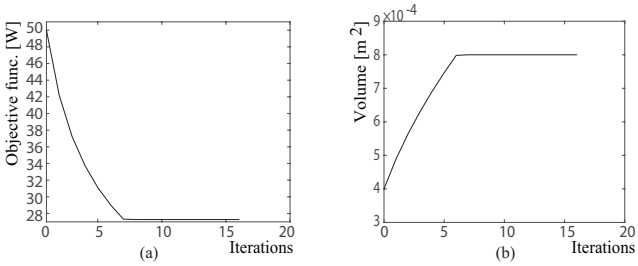

Figure 15 Iteration history of (a): objective function and (b): volume constraint with the normalization approach

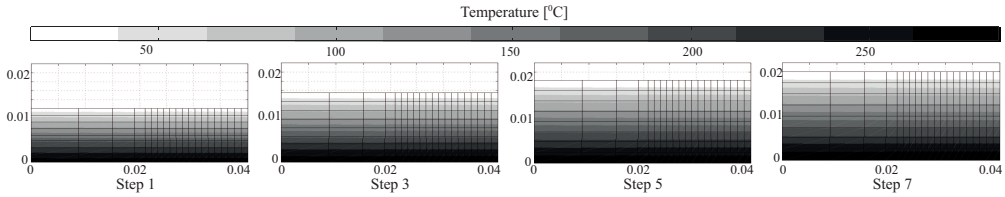

Figure 16 Evolution of the design shape with the normalization approach at selected steps throughout the optimization process and the corresponding temperature contour plot

method is globally more efficient since it generally requires fewer iterations to convergence.

8. Conclusions

In isogeometric shape optimization, the un-normalized search direction is strongly dependent on the discretization. In this paper, the effect of the discretization-dependency was analyzed. It was found that the un-normalized search direction was not consistent with the continuous steepest descent search direction. This problem was illustrated using a volume minimization problem with different discretizations. It was also found that the inconsistency originated from the discretization which induces a discrete quadratic norm to represent the continuous Euclidean norm. To fix this inconsistency, a standard normalization approach, which is used to find the steepest descent direction for quadratic norm problems, was proposed to obtain a consistent discretization -independent search direction. The standard approach requires solving a linear system of equations. Using the diagonally lumped mapping matrix (DLMM) and the partition of unity property of NURBS, two simpler normalization approaches, which do not require solving a linear system of equations, were proposed. The same volume minimization problem was presented to demonstrate the discretization-independence and equivalence of the proposed approaches, to within a relatively small numerical error, which eliminates the strong discretization-dependence of the discrete gradient. The normalization approach was tested in mechanical and thermal optimization problems, which overall provided a better performance and convergence characteristics. The proposed method can also be used for the traditional FE-based shape optimization to deal with the mesh- or parameterization-dependent solutions. It is also worth pointing out that the DLMM approach can also be used, more generally, to consistently discretize given functions (e.g., displacement boundary conditions) within the isogeometric analysis framework.

Acknowledgements. The authors would like to thank Prof. K.U. Bletzinger for the communication related to this work.

[1] T. J. Hughes, J. A. Cottrell, Y. Bazilevs, Isogeometric analysis: CAD, finite elements, NURBS, exact geometry and mesh refinement, Computer methods in applied mechanics and engineering 194 (39) (2005) 4135–4195.
[2] W. A. Wall, M. A. Frenzel, C. Cyron, Isogeometric structural shape optimization, Computer methods in applied mechanics and engineering 197 (33) (2008) 2976–2988.
[3] S. Cho, S.-H. Ha, Isogeometric shape design optimization: exact geometry and enhanced sensitivity, Structural and Multidisciplinary Optimization 38 (1) (2009) 53–70.
[4] A. P. Nagy, M. M. Abdalla, Z. Gürdal, Isogeometric sizing and shape optimisation of beam structures, Computer Methods in Applied Mechanics and Engineering 199 (17) (2010) 1216–1230.
[5] A. P. Nagy, M. M. Abdalla, Z. Gürdal, Isogeometric design of elastic arches for maximum fundamental frequency, Structural and Multidisciplinary Optimization 43 (1) (2011) 135–149.
[6] N. D. Manh, A. Evgrafov, A. R. Gersborg, J. Gravesen, Isogeometric shape optimization of vibrating membranes, Computer Methods in Applied Mechanics and Engineering 200 (13) (2011) 1343–1353.
[7] C. Long, A. Marsden, Y. Bazilevs, Shape optimization of pulsatile ventricular assist devices using fsi to minimize thrombotic risk, Computational Mechanics (2014) 1–12.
[8] A. P. Nagy, S. T. IJsselmuiden, M. M. Abdalla, Isogeometric design of anisotropic shells: Optimal form and material distribution, Computer Methods in Applied Mechanics and Engineering 264 (2013) 145–162.
[9] J. Kiendl, R. Schmidt, R. Wüchner, K.-U. Bletzinger, Isogeometric shape optimization of shells using semi-analytical sensitivity analysis and sensitivity weighting, Computer Methods in Applied Mechanics and Engineering 274 (2014) 148–167.
[10] X. Qian, O. Sigmund, Isogeometric shape optimization of photonic crystals via coons patches, Computer Methods in Applied Mechanics and Engineering 200 (25) (2011) 2237–2255.
[11] D. M. Nguyen, A. Evgrafov, J. Gravesen, Isogeometric shape optimization for electromagnetic scattering problems, Progress in Electromagnetics Research B 45 (2012) 117–146.
[12] M. Yoon, S.-H. Ha, S. Cho, Isogeometric shape design optimization of heat conduction problems, International Journal of Heat and Mass Transfer 62 (2013) 272–285.
[13] P. Nørtoft, J. Gravesen, Isogeometric shape optimization in fluid mechanics, Structural and Multidisciplinary Optimization 48 (5) (2013) 909–925.
[14] B.-U. Park, Y.-D. Seo, O. Sigmund, S.-K. Youn, Shape optimization of the stokes flow problem based on isogeometric analysis, Structural and Multidisciplinary Optimization 48 (5) (2013) 965–977.
[15] S.-H. Ha, K. Choi, S. Cho, Numerical method for shape optimization using T-spline based isogeometric method, Structural and Multidisciplinary Optimization 42 (3) (2010) 417–428.
[16] Z.-P. Wang, S. Turteltaub, Isogeometric shape optimization for quasi-static processes, International Journal for Numerical Methods in Engineering, accepted.
[17] K. Li, X. Qian, Isogeometric analysis and shape optimization via boundary integral, Computer-Aided Design 43 (11) (2011) 1427–1437.
[18] M.-J. Choi, S. Cho, A mesh regularization scheme to update internal control points for isogeometric shape design optimization, Computer Methods in Applied Mechanics and Engineering 285 (2015) 694–713.
[19] X. Qian, Full analytical sensitivities in NURBS based isogeometric shape optimization, Computer Methods in Applied Mechanics and Engineering 199 (29) (2010) 2059–2071.
[20] B. Koo, M. Yoon, S. Cho, Isogeometric shape design sensitivity analysis using transformed basis functions for Kronecker delta property, Computer Methods in Applied Mechanics and Engineering 253 (2013) 505–516.
[21] C. Le, T. Bruns, D. Tortorelli, A gradient-based, parameter-free approach to shape optimization, Computer Methods in Applied Mechanics and Engineering 200 (9) (2011) 985–996.
[22] F. Daoud, M. Firl, K. Bletzinger, Filter techniques in shape optimization with cad-free parametrization, in: Proceedings of 6th World Congress of Structural and Multidisciplinary Optimization, Citeseer, 2005.
[23] H. Azegami, S. Fukumoto, T. Aoyama, Shape optimization of continua using NURBS as basis functions, Structural and Multidisciplinary Optimization 47 (2) (2013) 247–258.
[24] A. Inzarulfaisham, H. Azegami, Solution to boundary shape optimization problem of linear elastic continua with prescribed natural vibration mode shapes, Structural and Multidisciplinary Optimization 27 (3) (2004) 210–217.
[25] H. Azegami, K. Takeuchi, A smoothing method for shape optimization: traction method using the robin condition, International journal of computational methods 3 (01) (2006) 21–33.
[26] M. Shimoda, J. Tsuji, H. Azegami, Non-parametric shape optimization method for thin-walled structures under strength criterion, Computer aided optimum design in engineering X. WIT Press, Southampton (2007) 179–188.

[27] S. Riehl, J. Friederich, M. Scherer, R. Meske, P. Steinmann, On the discrete variant of the traction method in parameter-free shape optimization, Computer Methods in Applied Mechanics and Engineering.
[28] K.-U. Bletzinger, M. Firl, J. Linhard, R. Wüchner, Optimal shapes of mechanically motivated surfaces, Computer methods in applied mechanics and engineering 199 (5) (2010) 324–333.
[29] M. Firl, R. Wüchner, K.-U. Bletzinger, Regularization of shape optimization problems using FE-based parametrization, Structural and Multidisciplinary Optimization 47 (4) (2013) 507–521.
[30] V. Braibant, C. Fleury, Shape optimal design using B-splines, Computer Methods in Applied Mechanics and Engineering 44 (3) (1984) 247–267.
[31] W. Zhang, D. Wang, J. Yang, A parametric mapping method for curve shape optimization on 3d panel structures, International Journal for Numerical Methods in Engineering 84 (4) (2010) 485–504.
[32] L. Espath, R. Linn, A. Awruch, Shape optimization of shell structures based on NURBS description using automatic differentiation, International Journal for Numerical Methods in Engineering 88 (7) (2011) 613–636.
[33] D. Wang, W. Zhang, A bispace parameterization method for shape optimization of thin-walled curved shell structures with openings, International Journal for Numerical Methods in Engineering 90 (13) (2012) 1598–1617.
[34] S. Cai, W. Zhang, J. Zhu, T. Gao, Stress constrained shape and topology optimization with fixed mesh: A B-spline finite cell method combined with level set function, Computer Methods in Applied Mechanics and Engineering 278 (2014) 361–387.
[35] L. Piegl, W. Tiller, The NURBS Book (2Nd Ed.), Springer-Verlag New York, Inc., New York, NY, USA, 1997.
[36] J. A. Cottrell, T. J. Hughes, Y. Bazilevs, Isogeometric analysis: toward integration of CAD and FEA, John Wiley & Sons, 2009.
[37] S. Boyd, L. Vandenberghe, Convex optimization, Cambridge university press, 2009.
[38] W. Böhm, G. Farin, J. Kahmann, A survey of curve and surface methods in CAGD, Computer Aided Geometric Design 1 (1) (1984) 1–60.
[39] K. K. Choi, N.-H. Kim, Structural sensitivity analysis and optimization 1: linear systems, Vol. 1, Springer, 2006.